Fluid Phase Equilibria 300 (2011) 182–187

Contents lists available at ScienceDirect

Fluid Phase Equilibria

journal homepage: www.elsevier.com/locate/fluid

Effect of pore morphology on vapor–liquid phase transition and crossover behavior of critical properties from 3D to 2D

Sudhir K. Singh, Jayant K. Singh*

Department of Chemical Engineering, Indian Institute of Technology Kanpur, Kanpur 208016, India

ARTICLE INFO

Article history:
Received 6 May 2010
Received in revised form 11 October 2010
Accepted 12 October 2010
Available online 20 October 2010

Keywords:
Confined fluid
Phase transition
Crossover behavior
Critical point

ABSTRACT

Grand-canonical transition-matrix Monte Carlo (GC-TMMC) simulation, is used to investigate the effect of pore shape and surface-fluid strength on the vapor–liquid phase transition and crossover behavior of critical properties from 3D to 2D of a square well (SW) fluid. We present the vapor–liquid coexistence phase diagram in hard and attractive cylindrical pores of varying slit width from 4 to 50 molecular diameters. This investigation indicates that having same pore shape but different surface nature can significantly alter the coexistence envelopes and hence the critical point. Critical temperature is found to approach the 3D bulk value monotonically irrespective of the pore shape and surface nature. However, the rate of approach of critical point towards the 3D bulk value decreases as the effective confinement increases. On the other hand, approach of pore critical density towards the bulk 3D value follows a non-monotonic path, irrespective of pore shape and surface strength. Interestingly, with the same pore shape, attractive wall surface follows an opposite trend to approach the bulk critical density as compared to that of hard wall surface. Crossover from 3D to 2D behavior in the hard cylindrical pores is observed around 28 molecular diameters, which is significantly larger than that observed by earlier workers for hard and attractive slit pores.

1. Introduction

In past decades numerous studies on porous materials with variety of pore geometries have been performed [1]. It has been observed that regardless of geometry, fluids confined in nano-pore sizes exhibit minimal to significant deviations from bulk thermophysical and structural properties at the same thermodynamic conditions [2–4]. The properties of confined fluids are determined particularly by their spatial density distribution, which is caused not only by the presence of solid surfaces and their geometry but also by the coexistence of phases of different densities. This knowledge is also of crucial importance for the interpretation of experimental data on fluid properties in pores. Using the available experimental techniques some coexistence curves were estimated from adsorption measurements of fluids in porous glasses [5] and ordered mesoporous silica materials [6,7]. In the aforesaid studies, an increase in the critical density and narrowing of two-phase region were observed. Additionally, these experimental studies also report an estimate of the shift in the pore critical temperature with respect to the bulk critical temperature. The shift of the pore critical temperature is reported to increase with decreasing pore sizes [8,9]. However, different experimental methods to define the disappearance of the phase transition resulted in significantly different values of shift in critical temperature for pores of similar size [6–8]. Undoubtedly, these experimental studies of the coexistence properties of fluids in porous materials indicate certain changes in the critical parameters of fluids with respect to that in the bulk phase; however, detailed and systematic studies are strongly limited by the available experimental techniques.

With the advent of efficient algorithms and theoretical techniques several studies of first order phase transition in a single pore have been reported using theory [10] and computer simulations [11–15]. Some recent molecular simulation investigations [16–21] on vapor–liquid phase transitions, interfacial properties and critical point shift on model fluids, such as square-well, Lennard–Jones and exponential-6, in slit pore geometries show interesting non-monotonic dependence on surface characteristics and degree of confinement. Similarly, Zhang and Wang found the non-monotonic behavior in the critical temperature shift in a cylindrical pore for various wall–fluid and fluid–fluid interaction strengths, using DFT calculations [22]. On the other hand, the authors observed monotonic behavior of critical density in a cylindrical pore with wall–fluid interaction. However, crossover behavior of critical point from 3D to 2D is not studied in cylindrical pores. In the current work, we focus on this aspect and investigate the vapor–liquid phase transition in cylindrical pores.

In a recent investigation [23], using canonical Monte Carlo simulations, vapor–liquid equilibrium of square-well fluid confined in

* Corresponding author.
E-mail address: jayantks@iitk.ac.in (J.K. Singh).

0378-3812/$ – see front matter © 2010 Elsevier B.V. All rights reserved.
doi:10.1016/j.fluid.2010.10.014

a single cylindrical pore with repulsive surface, have been studied. In that investigation two different coexistence densities, one at the pore centre and another at the wall surface were defined and it is demonstrated that at pore centre the saturated liquid density approaches to that of the bulk fluid as the diameter of the cylindrical pore increases. However, at the pore wall, the opposite behavior is observed. Moreover, it is expected that fluid confined in attractive pore will show inhomogeneities in its structure and several layers in the density profile will be observed. In this context, one can define separate vapor–liquid coexistence densities for each layer and hence separate vapor–liquid phase diagram corresponding to each layer. However, from experiment point of view [9] with material like MCM-41, which has well defined cylindrical pores, it is extremely difficult to capture the phase transition or pore critical temperature of different layers in a single cylindrical pore (same would be true for slit pore materials). Hence, for such applications it might be of significant interest to look at the average vapor–liquid phase transition and a global pore critical temperature in a single cylindrical pore, which further can be helpful to verify the experimental data with various systems.

This work is primarily to observe the surface and confinement driven changes in average vapor-like and average liquid-like coexistence densities of an entire cylindrical pore system, instead of looking at the local coexistence densities of different layers. This is our current objective for this work with a square-well fluid in a single cylindrical pore of repulsive and attractive surfaces of pore diameter varying from 3 to 50 molecular diameters. We also report a comparison of the results obtained in this work for cylindrical pores with that of slit pores studied earlier by us [19]. Further, we investigated the effect of pore shape and its surface nature on 3D to 2D crossover behavior of the confined fluid. The paper is organized as follows. Section 2 outlines the potential models and simulation details. In Section 3, we present the results of our investigation, and Section 4 concludes the study.

2. Potential models and simulation details

We have employed grand-canonical transition matrix Monte Carlo (GC-TMMC) simulation to calculate vapor–liquid phase diagram. The method is described in detail elsewhere [24]. In this work, fluid–fluid interaction, attractive wall–fluid and hard wall–fluid interaction are represented by the following square-well and hard-wall potentials:

$$u_{ff}(r) = \begin{cases} \infty, & 0 < r < \sigma_{ff} \\ -\varepsilon_{ff}, & \sigma_{ff} \le r < \lambda_{ff}\sigma_{ff} \\ 0, & \lambda_{ff}\sigma_{ff} \le r \end{cases},$$

$$u_{wf}(R) = \begin{cases} \infty, & R > R_c - \sigma_{ff}/2 \\ 0, & R < R_c - \sigma_{ff}/2 \end{cases},$$

$$u_{wf}(R) = \begin{cases} \infty, & R > R_c - \sigma_{ff}/2 \\ -\varepsilon_{wf}, & R_c - \lambda_{wf}\sigma_{ff} \le R \le R_c - \sigma_{ff}/2 \\ 0, & R < R_c - \lambda_{wf}\sigma_{ff} \end{cases}, \quad (1)$$

where r is the inter-particle separation distance, R is the radial distance of the particle from the central axis of the cylinder, R_c is the radius of cylinder, $\lambda_{ff}\sigma_{ff}$ is the fluid–fluid potential well diameter, ε_{ff} is the depth of the fluid–fluid potential well, σ_{ff} is the diameter of the fluid–fluid hard core, $\lambda_{wf}\sigma_{ff}$ is the fluid–wall potential well diameter, and ε_{wf} is the depth of the fluid–wall potential. All quantities reported in the rest of the article are made adimensional using characteristic energy, ε_{ff}, and length scale, σ_{ff}. For example, temperature is scaled by ε_{ff}/k. In this work, λ_{ff} is kept 1.5 and λ_{wf}, σ_{ff} and ε_{ff} each is kept 1.0 and for attractive surface ε_{wf} is taken as 4.0.

Critical parameters are estimated by using the coexistence data obtained via GC-TMMC simulation and the least square fit of the following scaling law [25]:

$$\rho_l - \rho_v = C\left(1 - \frac{T}{T_C}\right)^{\beta}, \quad (2)$$

where ρ_l, ρ_v,and T_C are coexistence liquid and vapor number densities, and critical temperature, respectively; C and β are fitting parameters. The parameter β is also known as order parameter critical exponent. The critical temperature, T_C, estimated from Eq. (2) is used to calculate the critical density, ρ_c, from the least square fit of the following equation:

$$\frac{\rho_l + \rho_v}{2} = \rho_c + D(T - T_C), \quad (3)$$

where D is a fitting parameter.

Critical pressure, P_c, is calculated using the least square fitting of the saturation pressure data obtained from the GC-TMMC simulations to the following expression, which has similar form as the Antoine equation:

$$\ln P_c = A - \frac{B}{T_C}, \quad (4)$$

where A and B are fitting parameters.

The saturated R-density profiles (profiles in the radial direction of cylinder), ρ_R, are obtained by recording $\rho(N,R)$ for each particle number sampled during GC-TMMC simulations. Coexistence density profiles are finally calculated using the following expression below:

$$\rho(R)_{\text{vapor/liquid}} = \frac{\sum_{i \in \text{vapor/liquid}} \Pi_C(i)\rho(i,R)}{\sum_{i \in \text{vapor/liquid}} \Pi_C(i)}, \quad (5)$$

where Π_C is the coexistence probability density distribution obtained from the application of histogram reweighting technique [26] on the transition matrix generated from the GC-TMMC simulation.

In this work, we also performed simulations in hard slit pores for the completeness in our comparison of the results between two different pore shapes. All simulations were conducted in grand-canonical ensemble with 30% displacement and 70% insertion/deletion moves. Although, periodic boundary conditions were implemented in the unconfined directions but to reduce any significant finite-size effect [27] of simulation cell size, on the coexistence properties, the maximum numbers of particles in the simulation cell were varied from 800 to 28,600 depending on the pore shape, size and nature of the surface. Critical exponent, β, obtained for cylindrical pores varies from around 0.47 for the largest pore diameter to the value of around 0.16, for the smallest pore diameter of 3 molecular diameters studied in the current work. Three independent runs are conducted to obtain the statistical error in critical properties. The errors in pore critical temperature (T_{cp}), critical density (ρ_{cp}) and critical pressure (P_{cp}) for the hard wall, are less than 0.3%, 0.6% and 0.7%, respectively; whereas, for the attractive wall corresponding errors are less than 0.35%, 0.75% and 0.5%, respectively.

3. Results and discussion

3.1. Effect of surface nature on vapor–liquid phase diagram

Fig. 1(a) and (b) shows the vapor–liquid phase diagram plot of a square-well fluid confined in hard and attractive cylindrical pore of pore diameter varying from 3 to 50 and 4 to 50 molecular

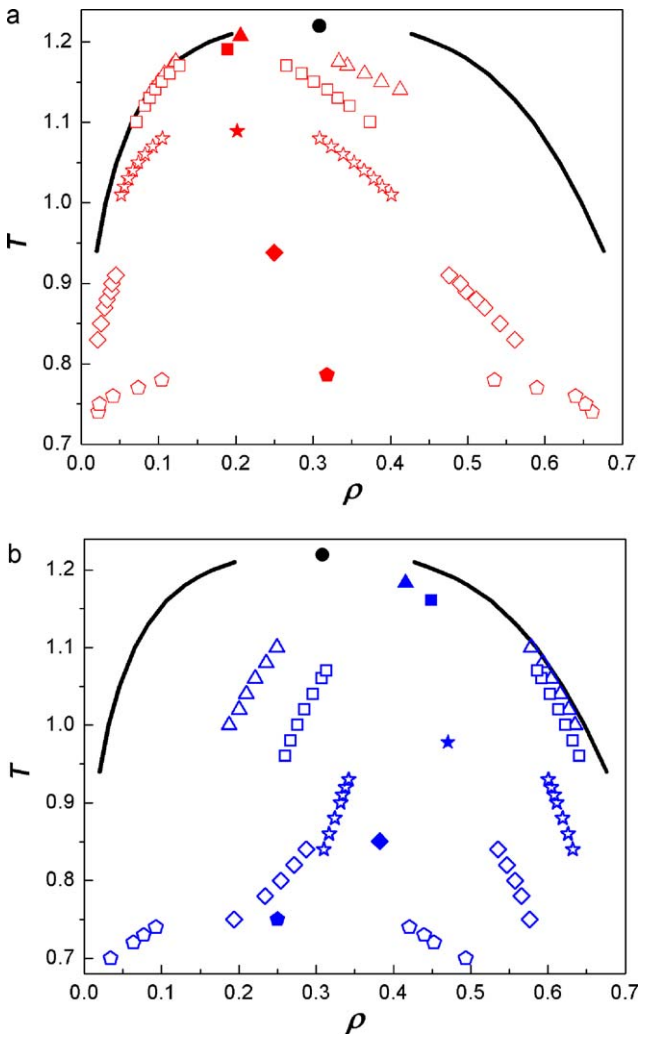

Fig. 1. Temperature–density vapor–liquid coexistence curve for a square-well fluid in the cylindrical pore confinement of hard and attractive surfaces is shown in (a) and (b), respectively. Solid curve represents the bulk coexistence envelope with the symbol filled circle as the bulk critical point [19]. Open and filled symbols represent the coexistence densities and corresponding critical point, respectively. Symbols triangle, square, star, diamond and pentagon represent the case with pore diameter, D = 50, 24, 10, 6 and 4, respectively.

diameters, respectively. Bulk vapor–liquid phase envelope is also included in plots of Fig. 1(a) and (b) to see the relative behavior of the phase coexistence envelopes. If we see the coexistence envelope of vapor branch of the fluid confined in hard wall cylindrical pore with pore diameter, D, 50–24 (see Fig. 1(a)) it shows insignificant differences with the bulk vapor phase branch. On the other hand, significant reduction is seen in the corresponding liquid density as compared to the bulk liquid phase densities. Coexistence envelope shrinks with reduction in D from 50 to 10, as also noted by earlier workers [23,28]. As D is decreased below 6 molecular diameters, comparative broadening in the phase coexistence envelope is seen from 6 to 3 molecular diameters for hard cylindrical pore. This relative broadening of coexistence envelope can be seen in Fig. 1(a) for D = 6 and 4. As expected, critical temperature continuously decreases with decrease in D; on the other hand, critical density shows non-monotonic trend and goes through a minima with increase in D before approaching the bulk value. Conversely, in attractive cylindrical pore, as shown in Fig. 1(b), coexistence envelope shows different behavior. Liquid phase densities in pores, with D = 50–24, are found to be comparatively closer to the bulk liquid phase densities, contrary to the corresponding hard wall case. However, vapor phase densities are far away from the corresponding bulk phase vapor densities, which is contrary to the hard wall behavior of the same pore diameter. Phase coexistence envelope shrinks with decrease in D till 6 molecular diameters and below 6 it starts broadening. This behavior is akin to that seen for the hard wall pores.

Critical temperature continuously decreases with the decrease in D as expected; however, critical density goes through a maximum with increase in D, before approaching the bulk value. Thus, the phase coexistence envelopes and corresponding critical point approach towards bulk phase envelopes and bulk critical point is highly sensitive to the surface nature even with the same shape of the pore.

3.2. Effect of pore shape on vapor–liquid phase diagram

Fig. 2 presents the phase coexistence envelope comparison of a fluid confined in pores of two different shapes, namely slit and cylinder, having same surface attraction. Phase coexistence comparison is shown for slit width (in case of slit pore) and pore diameter (in case of cylindrical pore) varying from 40 to 4 molecular diameters. For the studied slit widths and pore diameters, qualitative approach of coexistence envelopes and critical points of confined square-well fluid is nearly similar. On the other hand, the relative shift of coexistence density, away from the bulk phase coexistence densities in cylindrical pores is comparatively larger than that in the slit pores. This clearly suggests the greater confinement effect in cylindrical pores as compared to slit pore of same slit width or pore diameter and surface attraction. Fig. 2 also suggests that approach of pore critical point towards the bulk value is comparatively slower in cylindrical pores, for the same set of pore sizes. We have described the approach of the pore critical point towards the 3D bulk value, in more detail, in Section 3.4.

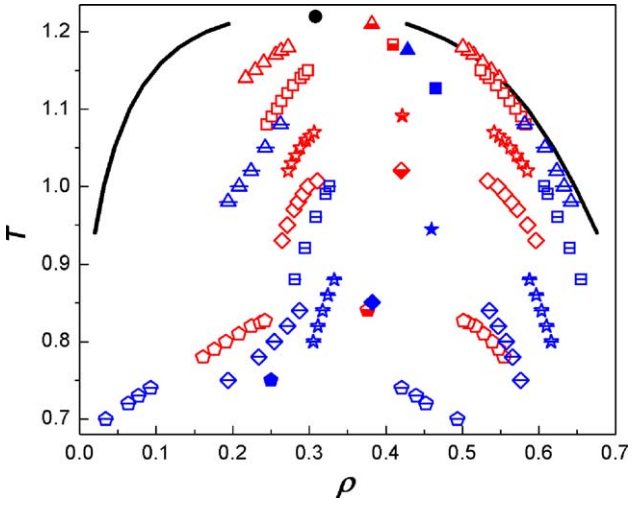

Fig. 2. Temperature–density vapor–liquid coexistence curve for a square-well fluid in attractive slit and cylindrical pores. Solid curves represent the bulk coexistence envelope with the symbol filled circle as the bulk critical point. Red colored open and half filled symbols represent the coexistence densities and corresponding critical point, respectively, of the fluid in attractive slit pores (data taken from Ref. [19]); blue colored open symbols with a horizontal cut and filled symbols represent the case of attractive cylindrical pores. Symbols triangle, square, star, diamond and pentagon represent the case with slit width, H (in slit pore) and pore diameter, D (in cylindrical pore) = 40, 16, 8, 6 and 4, respectively. Attractive strength of slit and cylindrical surfaces are same for all the cases. (For interpretation of the references to color in this figure legend, the reader is referred to the web version of the article.)

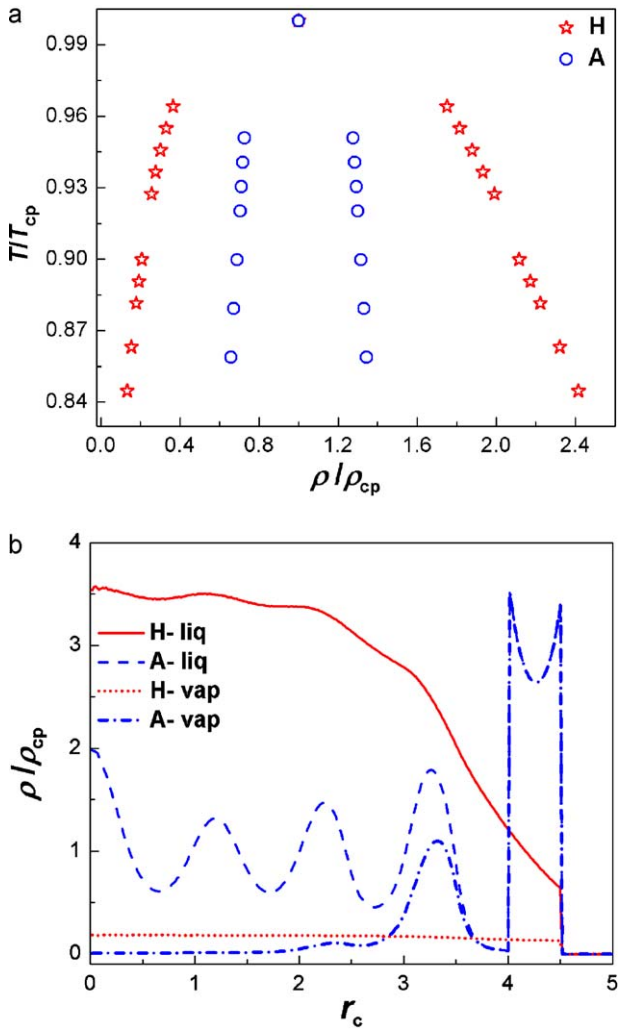

Fig. 3. Corresponding state plots of vapor–liquid coexistence envelopes in hard (H) and attractive (A) cylindrical pore of width $D = 10$ molecular diameters are shown in (a). Typical radial density (R-density) profiles of coexisting vapor and liquid phases are shown in (b) at a reduced temperature, $T/T_{cp} = 0.86$.

3.3. Corresponding state analysis of vapor–liquid phase diagram in cylindrical pore

Fig. 3(a) and (b) presents the corresponding state plot of the phase diagram and density profile, respectively, of the SW fluid confined in a hard (H) and attractive (A) cylindrical pore with $D = 10$. Similar corresponding state behavior is observed with other studied pore diameters in this work. Fig. 3(a) shows that nature of surfaces plays a significant role on the coexistence phase diagram even in the corresponding state plots. It is observed that at a given reduced temperature, T/T_{cp}, attractive cylindrical pore tends to increase the reduced vapor density and lowers the reduced liquid density. To understand this behavior of coexistence phase diagram, we evaluated the local R-density profiles of coexisting phases at a typical reduced temperature, $T/T_{cp} = 0.86$, for hard and attractive cylindrical surfaces. Fig. 3(b) shows the typical R-density profiles of the two coexisting phases, in attractive cylindrical pore, which clearly indicates two distinct layers in the vapor phase. On the other hand, no such layering is visible for hard cylindrical pore. Hence, average vapor density with attractive cylindrical pore is higher as compared to that for the case of hard cylindrical pore. Moreover, in the attractive cylindrical pore, near the pore surface it becomes difficult to separate out the two coexisting phases as can be seen from Fig. 3(b). Local liquid phase densities, throughout the pore diameter, in the hard cylindrical pore, are significantly larger than that seen in the attractive pore except near the pore surface. Near the surface of the attractive pore strong layering is observed and its density is significantly larger compared to that seen for the hard pore. The dominance of local liquid densities in the region away from surfaces of the hard cylinder is in fact resulted in higher average reduced liquid density as observed in Fig. 3(a).

3.4. Effect of pore shape and surface attraction on pore critical point approach to the bulk value

In Fig. 4(a)–(c), pore critical temperature T_{cp}, pore density ρ_{cp}, and pore critical pressure P_{cp} normalized by bulk critical temperature T_{cb}, critical density ρ_{cb}, and critical pressure P_{cb}, respectively, are plotted, against pore width (for slit pore) or pore diameter (for cylindrical pore). Table 1 summarizes all the critical data reported in Fig. 4. Fig. 4(a) shows that the surface nature and pore shape significantly affect the pore critical temperature, T_{cp}, and its approach to T_{cb}. Fluid in hard cylindrical pores approaches the 3D bulk critical temperature more rapidly compared to that seen for attractive cylindrical pores, for the same set of pore sizes. On the other hand, same fluid subjected under attractive slit pore, with the same surface attraction as that for cylindrical pore, approaches the bulk behavior much earlier than that seen in cylindrical pore with increase in the pore size. Fig. 4(b) presents the approach of pore critical density towards the bulk critical density. For all four studied cases, ρ_{cp} clearly displays the sign of approach towards the ρ_{cb}. Interestingly, ρ_{cp} in the hard slit and cylindrical pore shows entirely different behavior of its approach to the 3D bulk value as compared to that seen in the attractive slit and cylindrical pore. Moreover, the qualitative approach of ρ_{cp} towards ρ_{cb} is insensitive to the change in shape of pore with a constant surface attraction. On the other hand, with the same pore shape and different surface nature, significant difference even in qualitative approach is observed as depicted in Fig. 4(b). In Fig. 4(c), comparative approach of pore critical pressure, P_{cp}, towards the bulk value, P_{cb}, is shown. It is clear from Fig. 4(c) that in hard and attractive slit pore and hard cylindrical pore, P_{cp} shows the sign of approach to the bulk value with increase in slit width, H and pore diameter D. We do not report coexistence pressure for larger attractive cylindrical pores with $D > 16$ due to some numerical issues. Nonetheless, we expect P_{cp}/P_{cb}, in attractive cylindrical pore, to decrease with increase in pore diameter and approach to the bulk value akin to the behavior seen for attractive slit pores. More importantly, for a given fluid, qualitative approach of P_{cp} to the bulk value is similar for attractive pore irrespective of the studied pore geometry, and similar is the case with hard surfaces. On the other hand, with the same pore shape and different surface nature, significant difference even in qualitative approach of P_{cp} is observed as depicted in Fig. 4(c).

3.5. Effect of pore shape and surface attraction on the crossover behavior

In this work, with a square-well fluid, we studied the effect of pore shape and surface nature on 3D to 2D crossover behavior of the fluid confined in cylindrical pores as shown in Fig. 5. Fisher and Nakanishi [29] with the help of scaling arguments showed that the decrease in the critical temperature in larger pores should obey the relation, $(T_{cb} - T_{cp})/T_{cb} = kH^{-1/\nu}$, where ν is the critical exponent for the correlation length and k is a proportionality constant. To account for the strongly adsorbed layer on pore walls it is necessary to replace the true slit width H (in slit pore) or pore diameter D (in cylindrical pore), by a modified pore width or diameter, H_{eff} or D_{eff}, which accounts for t the adsorbed layers thickness that forms prior to capillary condensation. Using Ising 3D

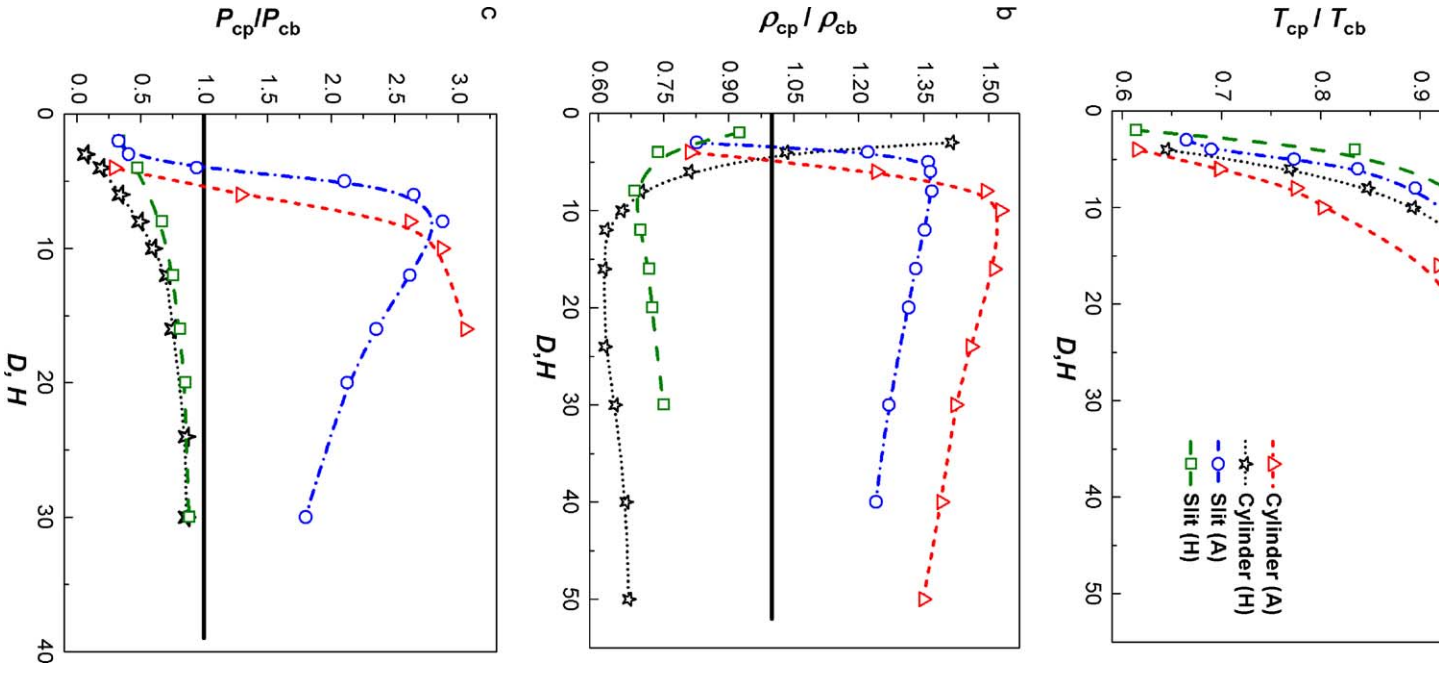

Fig. 4. The dependence of pore critical temperatures, critical density and critical pressure (all reduced by the corresponding bulk values) on pore diameter, D and slit width H is shown in (a)–(c), respectively, for hard (H) and attractive (A) slit and cylindrical pores. Attractive cylinder and slit surfaces have the same attraction strength. Thick horizontal solid line represents the 3D bulk value. Symbols in (b) and (c) have the same meaning as in (a). Curves along with symbols are shown just as a guide to eye.

Table 1
The adimensional T_c, ρ_c and P_c data of a square-well fluid in different types of pores of variable pore widths (in case of cylindrical pore, pore width is taken as the diameter of cylinder, D, and in slit pore, slit width, H) are tabulated. Symbol '–' indicates that the data is not reported. Numbers in parentheses indicate the 67% confidence limits of the last digit of the reported value. Critical point data of hard slit pores are taken from Refs. [16,17], except the data of pore width 16, 20 and 30 which is investigated in current work. Data of attractive slit pores are taken from Ref. [19].

Pore width	Cylindrical pore						Slit pore					
	Hard (H)			Attractive (A)			Hard (H)			Attractive (A)		
D, H	T_c	ρ_c	P_c	T_c	ρ_c	P_c	T_c	ρ_c	P_c	T_c	ρ_c	P_c
50	1.207(3)	0.2061(25)	–	1.188(4)	0.4154(3)		–	–		–	–	
40	1.200(2)	0.2044(3)	–	1.177(3)	0.4283(4)		–	–		1.209(2)	0.3816(3)	
30	1.195(2)	0.1967(2)	0.0824(3)	1.169(3)	0.4383(3)		1.204(2)	0.2309(4)	0.0844(2)	1.204(1)	0.3908(5)	0.1724(4)
24	1.190(4)	0.1894(5)	0.0822(2)	1.160(3)	0.4491(6)		–	–		–	–	
20	–	–	–	–	–		1.198(4)	0.2227(3)	0.0813(3)	1.193(2)	0.4048(6)	0.2039(5)
16	1.156(3)	0.1888(3)	0.0721(4)	1.126(4)	0.4656(4)	0.2933(6)	1.187(1)	0.2205(2)	0.0771(8)	1.183(2)	0.4099(3)	0.2258(3)
12	1.132(5)	0.1900(4)	0.0679(2)	–	–		1.177(3)	0.2143(5)	0.0720(5)	1.158(3)	0.4162(6)	0.2511(2)
10	1.089(3)	0.2015(7)	0.0575(3)	0.978(4)	0.4703(6)	0.2756(4)	–	–		–	–	
8	1.034(5)	0.2154(7)	0.0471(5)	0.945(2)	0.4597(4)	0.2513(3)	1.143(3)	0.2101(6)	0.0635(7)	1.091(4)	0.4214(4)	0.2760(3)
6	0.938(1)	0.2496(4)	0.0325(4)	0.851(2)	0.3821(5)	0.1234(2)	–	–		1.021(1)	0.4202(6)	0.2540(4)
5	–	–	–	–	–		–	–		0.9424(2)	0.4186(5)	0.2017(3)
4	0.786(2)	0.3178(5)	0.0181(4)	0.750(1)	0.2498(6)	0.0277(4)	1.015(1)	0.2265(2)	0.045(6)	0.841(2)	0.3758(5)	0.090(2)
3	0.622(3)	0.4355(4)	0.0062(3)	–	–		–	–		0.8099(2)	0.2543(6)	0.0385(4)
2	–	–	–	–	–		0.748(1)	0.2843(3)	0.0314(5)	0.745(2)	0.2849(4)	0.0311(6)

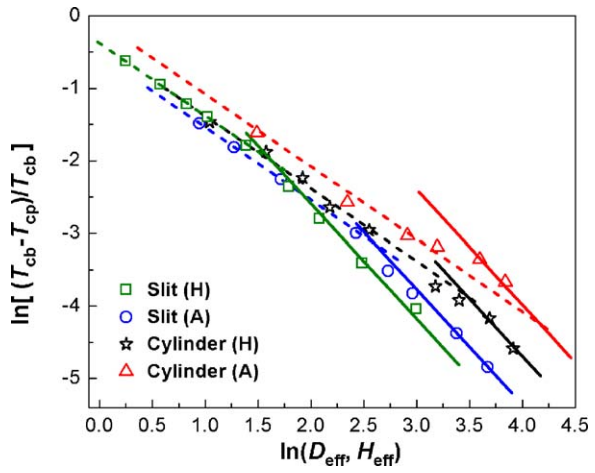

Fig. 5. Crossover from 3D to 2D of a square-well fluid in hard (H) slit (data taken from Ref. [17]), attractive (A) slit (data taken from Ref. [19]), hard and attractive cylindrical pores (current work) are shown. Correlation length critical exponent, ν, is represented by solid and dashed lines for 3D and 2D regimes, respectively.

(bulk) correlation length critical exponent $\nu(3D) = 0.63$, and Ising 2D correlation length critical exponent [30], $\nu = 1$, we have evaluated the effective layering thickness, t, of the adsorbed layer in the slit and cylindrical pore by fitting the logarithmic form of the relation, $(T_{cb} - T_{cp})/T_{cb} = k(H - t)^{-1/\nu}$. We observed in our earlier work [19] that in larger slit pore the layering thickness, t, is insignificant for both hard and attractive surfaces. However, for smaller slit pore with hard and attractive surfaces, t, is around 0.22 and 2.43, respectively. Similarly, in the cylindrical pore of hard surface, with larger pore diameter, t, is insignificant. However, for smaller cylindrical pore regime with hard and attractive surfaces, t is around 3.16 and 5.6, respectively. In Fig. 5, the relative critical temperature, $(T_{cb} - T_{cp})/T_{cb}$ is plotted as a function of the effective slit width, H_{eff} (i.e. $H - t$) or D_{eff} (i.e. $D - t$) on a log–log scale for the confined square well fluid in slit and cylindrical pores. It is observed in our earlier work [17,19] and also indicated from Fig. 5 that the crossover from 3D to 2D in hard and attractive slit pores occurs at around $H \sim 5$ and 14 molecular diameters, respectively. On the other hand, for the same fluid in hard cylindrical pore the crossover occurs at around 28 molecular diameters, which is significantly larger than that observed in the slit pore geometry. In addition, it appears from Fig. 5 that in the case of attractive cylindrical pore crossover from 3D to 2D probably will occur at around a pore diameter much larger than the pore diameters studied in the current work. Nevertheless, this investigation indicates that for a fluid, crossover behavior is significantly affected by the pore shape and surface field.

4. Conclusions

This work illustrates how the pore shape and its surface characteristics can alter the vapor–liquid phase equilibrium of a confined fluid, by taking a simple fluid, a square well fluid, and subjected in pores with diameter ranging from 3 to 50 molecular diameters. Phase coexistence envelope and critical properties are found to depend significantly on the pore shape and surface field. Approach of pore critical temperature to the 3D bulk value, with the increase of slit width or pore diameter, is significantly affected by pore shape and the surface nature. Moreover, approach of pore critical density towards bulk critical density differs qualitatively also, for same pore shape but different surface nature. On the other hand, the qualitative behaviors with different pore shape and same surface nature are near similar. These investigations suggest pore critical temperature approaches the bulk value monotonically irrespective of pore shape and the surface nature. However, approach of pore critical density towards the bulk critical density shows non-monotonic trend. In the current work, we have also studied the effect of pore shape and surface nature on 3D-to-2D crossover behavior of a square-well fluid. The current studies reveals that for a given fluid, onset of crossover from 3D to 2D-like behavior starts much earlier for attractive cylindrical pore followed by hard cylinder, attractive slit and hard slit pore, respectively. We observed that crossover behavior with hard slit pore, attractive slit pore and hard cylindrical pore occurs around 5, 14 and 28 molecular diameters, respectively, however, with attractive cylindrical pore it appears that the crossover pore size is much larger than the pore diameters studied in this work.

Acknowledgement

This work was supported by the Department of Science and Technology, Govt. of India (Grant Nos. SR/S3/CE/061/2009 and IR/S3/EU/005/2007).

References

[1] L.D. Gelb, K.E. Gubbins, R. Radhakrishnan, M. Sliwinska-Bartkowiak, Rep. Prog. Phys. 62 (1999) 1573.
[2] R. Evans, J. Phys.: Condens. Matter 2 (1990) 8989.
[3] R. Evans, A.O. Parry, J. Phys.: Condens. Matter 2 (1990) SA15.
[4] R. Zangi, J. Phys.: Condens. Matter 16 (2004) S5371.
[5] M. Tommes, G.H. Findenegg, Langmuir 10 (1994) 4270.
[6] S. Gross, G.H. Findenegg, Ber. Bunsenges. Phys. Chem. 101 (1991) 1726.
[7] W.D. Machin, Phys. Chem. Chem. Phys. 5 (2003) 203.
[8] K. Morishige, H. Fujii, M. Uga, D. Kinukawa, Langmuir 13 (1997) 3494.
[9] K. Morishige, M. Shikimi, J. Chem. Phys. 108 (1998) 7821.
[10] V. Privman, M.E. Fisher, J. Stat. Phys. 33 (1983) 385.
[11] G.S. Heffelfinger, F. Swol, K.E. Gubbins, Mol. Phys. 61 (1987) 1381.
[12] B.K. Peterson, K.E. Gubbins, G.S. Heffelfinger, U. Marini Bettolo Marconi, F. Swol, J. Chem. Phys. 88 (1988) 6487.
[13] L.D. Gelb, K.E. Gubbins, Phys. Rev. E 55 (1997) R1290.
[14] Z. Zhang, A. Chakrabarti, Phys. Rev. E 50 (1994) R4290.
[15] I. Brovchenko, A. Geiger, A. Oleinikova, J. Chem. Phys. 120 (2004) 1958.
[16] J.K. Singh, S.K. Kwak, J. Chem. Phys. 126 (2007) 24702.
[17] S. Jana, J.K. Singh, S.K. Kwak, J. Chem. Phys. 130 (2009) 214707.
[18] S.K. Singh, A. Sinha, G. Deo, J.K. Singh, J. Phys. Chem. C 113 (2009) 7170.
[19] S.K. Singh, A.K. Saha, J.K. Singh, J. Phys. Chem. B 114 (2010) 4283.
[20] H.L. Vortler, Collect. Czech. Chem. Commun. 73 (2008) 518.
[21] Y. Liu, A.Z. Panagiotopoulos, P.G. Debenedetti, J. Chem. Phys. 132 (2010) 144107.
[22] X. Zhang, W. Wang, Phys. Rev. E 74 (2006) 062601.
[23] Y.R. Mercado, P. Orea, S.L. Ramírez, Y. Duda, Physica A 388 (2009) 799.
[24] J.R. Errington, J. Chem. Phys. 118 (2003) 9915–9925.
[25] J.K. Singh, J. Adhikari, S.K. Kwak, Fluid Phase Equilibr. 248 (2006) 1–6.
[26] A.M. Ferrenberg, R.H. Swendsen, Phys. Rev. Lett. 61 (1988) 2635.
[27] H.L. Vortler, K. Schafer, W.R. Smith, J. Phys. Chem. B 112 (2008) 4656.
[28] I. Brovchenko, A. Geiger, A. Oleinikova, J. Phys.: Condens. Matter 16 (2004) S5345.
[29] M. Fisher, H. Nakanishi, J. Chem. Phys. 75 (1981) 5857.
[30] R. Evans, U.T.P. Marconi Marini Bettolo, J. Chem. Phys. 84 (1986) 2376.